CHEMISTRY
A European Journal

A Journal of
ChemPubSoc Europe

Accepted Article

Title: Micellized tris(bipyridine)ruthenium catalysts affording preparative amounts of hydrated electrons with a green light-emitting diode

Authors: Robert Naumann, Florian Lehmann, and Martin Goez

To be cited as: *Chem. Eur. J.* 10.1002/chem.201801955

Link to VoR: http://dx.doi.org/10.1002/chem.201801955

Supported by
ACES

WILEY-VCH

10.1002/chem.201801955

Micellized tris(bipyridine)ruthenium catalysts affording preparative amounts of hydrated electrons with a green light-emitting diode[†]

By Robert Naumann, Florian Lehmann and Martin Goez[*]

Abstract: *We have explored alkyl substitution of the ligands as a means to improve the performance of the title complexes in photoredox catalytic systems that produce synthetically useable amounts of hydrated electrons through photon pooling. Despite generating a super-reductant, these electron sources only consume the bioavailable ascorbate and are driven by a green light-emitting diode (LED). The substitutions influence the catalyst activity through the interplay of the quenching parameters, the recombination rate of the reduced catalyst* OER *and the ascorbyl radical across the micelle–water interface, and the quantum yield of* OER *photoionization. Laser flash photolysis yields comprehensive information on all these processes and allows quantitative predictions of the activity observed in LED kinetics, but the latter method provides the only access to the catalyst stability under illumination on the timescale of the syntheses. The homoleptic complex with dimethylbipyridine ligands emerges as the optimum that combines an activity twice as high with an undiminished stability in relation to the parent compound. With this complex, we have effected dehalogenations of alkyl and aryl chlorides and fluorides, hydrogenations of carbon–carbon double bonds, and self- as well as cross-couplings. All the substrates employed are impervious to ordinary photoredox catalysts but present no problems to the hydrated electron as a super-reductant. A particularly attractive application is selective deuteration with high isotopic purity, which is achieved simply by using heavy water as the solvent.*

1 Introduction

Using the hydrated electron $e_{aq}^{\bullet-}$ as a relay allows extending photoredox catalysis[1–6] to aqueous solutions with a vengeance: $e_{aq}^{\bullet-}$ provides the reducing power of metallic potassium yet is persistent enough to be scavenged near-quantitatively by mM concentrations of substrates (standard electrode potential E° and unquenched lifetime of $e_{aq}^{\bullet-}$, -2.9 V and 1–2 μs);[7] and in doing its work on the substrate it self-destructs without leaving a by-product.

In a recent communication,[8] we have presented the first photoredox catalytic system that generates $e_{aq}^{\bullet-}$ on a laboratory scale while being both user-friendly and sustainable through operating with a green light-emitting diode (LED) instead of a high-power laser[9] and consuming only a bioavailable sacrificial species. After an attempt at replacing the latter

[*]Robert Naumann, Florian Lehmann, Prof. Dr. Martin Goez,
Martin-Luther-Universität Halle-Wittenberg, Institut für Chemie, Kurt-Mothes-Str. 2, D-06120 Halle (Saale), Germany.
E-mail: martin.goez@chemie.uni-halle.de

[†]Supporting Information available: Comprehensive experimental details, absorption and emission spectra in the visible range, additional laser flash photolysis results, LED photolysis background information, and NMR spectra for the LED-induced transformations via $e_{aq}^{\bullet-}$. See DOI: ...

10.1002/chem.201801955

to accommodate a specific class of synthetic applications,[10] here we focus on improving the catalyst.

Our electron sources rely on the sequence absorption — reductive quenching — photoionization, which cycles a tris(bipyridine)ruthenium catalyst through its ground state GS, metal-to-ligand charge-transfer excited state MLCT, and one-electron reduced complex OER.[11] Schematic structural formulas of the catalyst and ligand are displayed as the insets of Figure 1; and the substitution pattern of the ligands has been compiled in Table 1, below, together with the substance abbreviations used throughout this work. The ubiquitous antioxidant and approved food additive ascorbate serves as the sacrificial donor. To increase its reductive ability, we employ it in the form of its dianion Asc^{2-}, which necessitates working in strongly basic solution (pH 12.7). Its radical $Asc^{\bullet-}$ is very unreactive; in particular, it hardly intercepts $e_{aq}^{\bullet-}$.[12]

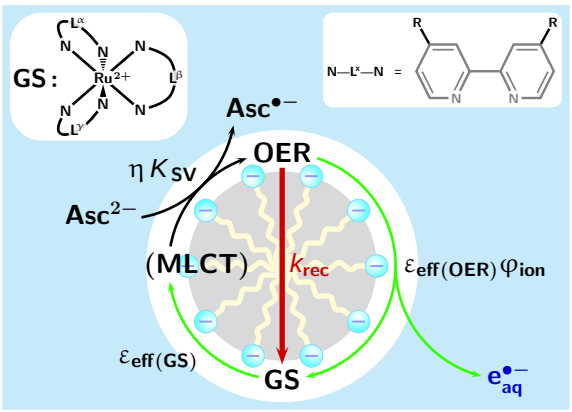

Figure 1: Introducing the green-light driven cyclic source of hydrated electrons $e_{aq}^{\bullet-}$. The schematic representation of the reaction mechanism allows comparative kinetic analysis of laser flash photolysis and preparative LED illumination. Light-driven steps are shown as green arrows. The micellized ruthenium catalyst (for its structural formula and that of the ligands, see the insets and Table 1) in its ground state GS undergoes photoinduced electron-transfer quenching via its metal-to-ligand charge-transfer excited state MLCT by the ascorbate dianion Asc^{2-} through the micelle–water interface. The obtained one-electron reduced form OER is then ionized by a second green photon, ejecting the hydrated electron $e_{aq}^{\bullet-}$ into the aqueous bulk and regenerating GS. All kinetic parameters needed for analysis are given at the reaction arrows. The storage-limiting recombination of OER and the ascorbyl radical $Asc^{\bullet-}$ is displayed in red.

The two-photon mechanism solves the problem that the energy of a single green photon (2.33 eV at 532 nm) does not suffice to eject $e_{aq}^{\bullet-}$ from any stable precursor molecule known to date.[13] Compared to its variant with post-ionization regeneration of the catalyst,[14] it also optimizes the storage of the energy bestowed by the first photon: OER as a "hidden" radical anion[15] does not undergo photophysical deactivation and is expected to decay predominantly by a second-order process, which is intrinsically more favourable than first-order deactivation; and compartmentalization by an anionic micelle augments this benefit considerably.[8]

When the second photon arrives after the "expiry date" of the stored first photon, no photoionization is possible. Hence, the storage losses by the bimolecular recombination of OER and $Asc^{\bullet-}$ fundamentally limit the $e_{aq}^{\bullet-}$ production at the low photon densities an LED delivers. As a strategy to minimize this recombination, we have increased the micellar shielding of the catalyst through substituting the ligands with alkyl groups in this work. We investigate the consequences of these modifications on short and long timescales, by laser flash photolysis and by the kinetics under LED illumination, relegating all experimental

details to Section 1 of the Supplementary Information (hereafter abbreviated to as SI–1, etc.) for conciseness. This comparative study pays heed to recently voiced concerns that mechanistic and kinetic studies on photoredox catalytic systems are much too scarce.[16–18]

As will emerge, no monocausal relationship between the structure of the catalyst and its performance in an $e_{aq}^{\bullet-}$ source exists, especially because the activity (i.e., the maximum rate at which $e_{aq}^{\bullet-}$ can be produced) is not the only property that counts; equally important is the catalyst stability under long-time illumination. This duality is also the reason why laser flash photolysis does not provide a complete picture but needs to be complemented by the LED kinetics. Our approach has resulted in identifying a significantly better catalyst; and we will demonstrate the successful application of this catalyst to a number of synthetic procedures on substrates that are extremely difficult to reduce but are readily attacked by $e_{aq}^{\bullet-}$.

2 Results and discussion

2.1 Mechanism and kinetics

2.1.1 Laser flash photolysis

Our 532 nm laser excites the lowest-energy band of GS (SI–2.2) at its red edge. When Ru(II) polypyridine complexes have absorbed a photon in the visible range, their long-lived MLCT excited states are formed by intersystem crossing within sub-ps.[15] During ns laser pulses, stimulated emission is thus noncompetitive such that a pulse of sufficient intensity can achieve complete conversion of GS into the luminescent MLCT. The left inset of Figure 2a demonstrates that we can drive our systems well into this limit with our setup.

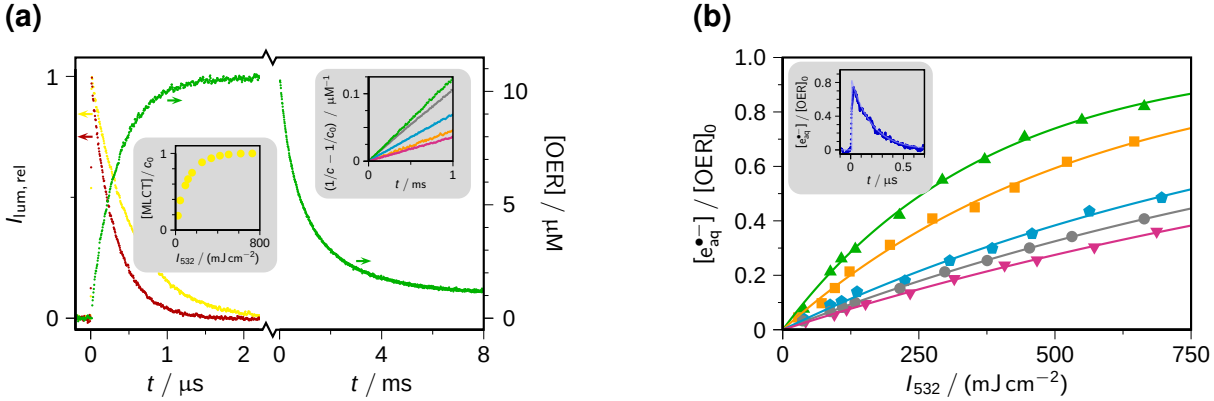

Figure 2: Characterizing the system of Figure 1 by laser flash photolysis. Common experimental parameters, 50 μM catalyst in 50 mM aqueous SDS at pH 12.7, 75 mM Asc^{2-} except for the yellow curve and left inset in graph (a). Catalyst (see Table 1) colour codes and symbols, where applicable: RuBpy, gray, circles; RuDmb, green, triangles; RuTbb, orange, squares; RuMdnb, cyan, pentagons; RuBdnb, magenta, inverted triangles. Graph (a), single-flash experiments on OER formation and decay. The main plot displays, on two timescales as indicated by the arrows at the curves, the unquenched (yellow) and quenched (red) luminescence and the OER concentration upon quantitative excitation (flash intensity, 728 mJ cm^{-2}) of RuDmb; left inset, MLCT concentration, from the unquenched luminescence intensity directly after the flash, as function of the excitation intensity; right inset, linearization demonstrating the bimolecular recombination of OER and $Asc^{\bullet-}$ for all catalysts. Graph (b), two-flash experiments (first flash, fixed intensity for quantitative excitation of GS; 5 μs delay for reaching the quenching end point; second flash, variable intensity I_{532}) for determining the $e_{aq}^{\bullet-}$ yield from OER; inset, $e_{aq}^{\bullet-}$ trace obtained from RuDmb at the maximum I_{532}, and superimposed best-fit first-order decay (rasterized curve).

We found strictly monoexponential decays of MLCT in the micellar solutions (SI–3.1). The unquenched lifetimes τ_0 have been compiled in Table 1. In the microheterogeneous medium, τ_0 is noticeably longer than in water, indicating that in all our experiments the complexes are completely micelle-bound. There is no discernible correlation between the — with 720 ns ± 25 % generally similar — values of τ_0 and the lipophilicity of the catalyst.

The expected quenching of MLCT by Asc^{2-} manifests itself by a shortening of the MLCT lifetime; and the MLCT decay is now accompanied by a rise of the OER absorption with the same rate (see, left half of Figure 2a). The MLCT decay remains monoexponential (SI–3.1) and exhibits the same initial amplitude as in the absence of Asc^{2-}, which identifies the quenching by the strongly hydrophilic dianion as a purely dynamic process across the micelle–water interface. Table 1 lists the quenching rate constants k_q; the dependence on the alkyl substituents will be discussed below.

Table 1: Investigated complexes: abbreviations and substitution pattern; standard electrode potentials; and photokinetic parameters obtained by laser flash photolysis.

catalyst	substituents R in ligand [a]			E° [b]	τ_0 [c]	k_q	η	k_{rec}	φ_{ion}
abbreviation	L^{α}	L^{β}	L^{γ}	[V]	[ns]	[10^7 $M^{-1}s^{-1}$]		[10^7 $M^{-1}s^{-1}$]	[%]
RuBpy	H	H	H	−1.07 [19]	830(620)	5.6	0.64	11	1.1
RuDmb	Me	Me	Me	−1.21 [19]	541(300)	1.8	0.55	12	2.3
RuTbb	*tert*-Bu	*tert*-Bu	*tert*-Bu	−1.20 [20]	880(380)	0.63	0.49	4.6	0.90
RuMdnb	H	H	*n*-C_9H_{19}	−1.13 [d]	856(490)	2.9	0.51	7.0	1.1
RuBdnb	H	*n*-C_9H_{19}	*n*-C_9H_{19}	−1.17 [e]	725(n/a) [f]	1.4	0.52	3.6	0.69

[a] See ligand structure in Figure 1. [b] Standard electrode potential of the couple GS/OER in acetonitrile. [c] Values in homogeneous aqueous solution given in brackets. [d] Unavailable value approximated by the average of E° for (4,4′-dimethyl-2,2′-bipyridine)-bis-(2,2′-bi-pyridine)-ruthenium-(II) [19] and (4,4′-di-*tert*-butyl-2,2′-bipyridine)-bis-(2,2′-bipyridine)-ruthenium-(II) [20]. [e] Unavailable value approximated by the average of E° for bis-(4,4′-dimethyl-2,2′-bipyridine)-(2,2′-bipyridine)-ruthenium-(II) [19] and bis-(4,4′-di-*tert*-butyl-2,2′-bipyridine)-(2,2′-bipyridine)-ruthenium-(II) [20]. [f] Insufficiently soluble and self-associating in water.

Neither Asc^{2-} nor its radical $Asc^{\bullet-}$ absorb in the green; and all our catalysts possess an isosbestic point between GS and MLCT around 510 nm, which almost coincides with the maximum of the OER band (SI–2.4). Hence, that isosbestic wavelength permits not only isolated but also very sensitive monitoring of OER. We calibrated the OER spectra by using a quencher (4-methoxy phenolate) that affords a more favourably absorbing radical than $Asc^{\bullet-}$ and by exploiting an isosbestic point between GS and OER that occurs in the vicinity of 410 nm for all our complexes. Details are again found in SI–2.4. In conjunction with the quantitative conversion of GS into MLCT and the Stern–Volmer constant K_{SV} calculated from k_q and τ_0,

$$K_{SV} = \left(1 + 1/(k_q \tau_0 [Asc^{2-}])\right)^{-1} \quad (1)$$

the absolute OER concentrations after the quenching directly yield the efficiency η of OER formation. The resulting values have also been included in Table 1. They are seen to be very similar with the exception of RuBpy, for which η is about 20 % higher.

The right half of Figure 2a focuses on the decay of OER, which takes place on a disparately longer timescale. The clear second-order kinetics during the first ms — as established by the linearizations in the inset, which directly give the values of k_{rec} in Table 1 — naturally suggest interpreting this decay as the expected recombination of OER and the quenching by-product

$Asc^{\bullet-}$. This identification as a reaction between unlike species formed in equal amounts is validated by different decay rate constants k_{rec} when OER of the same catalyst is accessed with different quenchers, e.g., Asc^{2-} *vs.* the urate dianion.[10] As a secondary effect that only becomes visible in wider observation windows, we found an apparent decrease of the recombination rate constant over time. We attribute this to the additional gradual removal of the recombination partner $Asc^{\bullet-}$ by its disproportionation.[21] Corroboration of this explanation was obtained by halving the initial radical concentration through a lower laser intensity: this led to a much later onset of the deceleration (SI–3.2). Even though a complete kinetic description is hopeless on account of the highly complex secondary chemistry of $Asc^{\bullet-}$,[21] the disproportionation is obviously beneficial to an LED driven electron generator because it prolongs the availability of OER for absorbing the ionizing photon; in other words, because it increases the ”shelf life” of the energy stored in the system by the first photon, which becomes more and more crucial when the photon flux is lowered.

The emission spectra (SI–2.3) confine the MLCT energies to an interval only ± 0.03 eV wide around the value for RuBpy (2.12 eV)[15]; the standard electrode potentials E° (Table 1) are clustered in the narrow range -1.14 ± 0.07 V; and E° of the couple $Asc^{\bullet-}/Asc^{2-}$ is +0.05 V.[21] Hence, both the quenching of MLCT by Asc^{2-} and the recombination of OER and $Asc^{\bullet-}$ are strongly exergonic, with relatively small variations of the driving force by the ligands. This suggests the accessibility of the micellized complex as the major influence on the kinetics. Most exposed in the series RuBpy, RuMdnb, and RuBdnb is an unsubstituted bipyridine ligand; rising lipophilicity of the other ligands will draw the complex more into the interior of the micelle. Comparing quenching and recombination, the Coulombic effects partly cancel: the dication MLCT sticks out more into the polar Stern layer than does the monocation OER, but the quenching dianion Asc^{2-} is repelled more strongly by the negative surface charge of the micelle than is the recombining monoanion $Asc^{\bullet-}$. Consistent with this reasoning, these three complexes exhibit a proportionality between k_{rec} and k_q with the ratio k_{rec}/k_q only about half as large as the variation of each rate constant in that series (SI–3.3). For the homoleptic complexes RuDmb and RuTbb, the exposed ligand is also different, and shielding by the aliphatic substituents can additionally modulate the accessibility to Asc^{2-} and $Asc^{\bullet-}$. Hence, stronger effects are expected, and the constant of proportionality is indeed found to be more than twice as large as the individual variability.

The pivotal step of the electron source of Figure 1 is the ionization of OER with a (second) green photon, which excites OER practically at the maximum of its lowest-energy band (SI–2.4). We studied that process by two-pulse experiments, in which we used a high-intensity first pulse to achieve quantitative formation of MLCT, ensured completion of the OER generation by an interpulse delay of 5 μs (compare, left half of Figure 2a), and varied the intensity of the second pulse. Furthermore, we observed $e_{aq}^{\bullet-}$ in isolation by difference experiments without and with N_2O saturation (SI–1), a procedure that succeeds even in the presence of strongly absorbing other transients and/or ”pathological” background artifacts in micellar systems.[13,22]

The $e_{aq}^{\bullet-}$ decay (for a representative trace, see the inset of Figure 2b) is monoexponential, and a catalyst-independent lifetime of 194 ns rules out an influence of the ruthenium complexes on the further fate of $e_{aq}^{\bullet-}$ after its generation. This is consistent with our earlier

investigations,[8,9,14] which pinpointed the capture of $e^{\bullet-}_{aq}$ by residual ascorbate monoanion $HAsc^-$ as the lifetime-limiting factor in the absence of deliberately added scavengers. The pK_a of $HAsc^-$ is 11.74;[21] hence, the $HAsc^-$ concentration is about 7.5 mM in the experiments of this work. Although the elusive[23] product of the reaction between $e^{\bullet-}_{aq}$ and $HAsc^-$ interferes neither spectroscopically nor mechanistically with our desired $e^{\bullet-}_{aq}$-induced syntheses, it lowers the $e^{\bullet-}_{aq}$ utilization through (fortunately only inefficient) kinetic competition. The convolution of the fast decay with the 5 ns generating pulse noticeably rounds the cusp ideally expected for the $e^{\bullet-}_{aq}$ trace. To obtain the true initial heights, we therefore extrapolated the electron decays back to the center of the laser flash, as seen superimposed on the trace.

The main plot of Figure 2b displays the intensity dependences of the $e^{\bullet-}_{aq}$ yield. Their initial linear rise confirms the expected monophotonic ionization of OER; but this is only the first-order term of the dependence over the full range of intensities, a saturation curve $1 - \exp(-\kappa I)$ whose parameter κ is proportional to φ_{ion} and to the extinction coefficient of OER as the only catalyst-specific quantities.[24] The values of φ_{ion} extracted with the calibrated OER spectra of SI–2.4 have been collected in Table 1. At first glance, their trend seems to reflect a competition between alkyl substitution facilitating the ionization through a higher energy of OER and impeding it through a "deeper" localization of OER inside the micelle. However, the much more electron-rich yet less lipophilic tris-(4,4′-dimethoxy-2,2′-bipyridine)-ruthenium(II) disproves this explanation: although OER of this derivative ($E^\circ(\mathrm{GS}/\mathrm{OER}) = -1.25$ V)[25] should be the best $e^{\bullet-}_{aq}$ emitter on both counts, we found φ_{ion} to be only 1.6 % (and the quenching parameters so unfavourable as to render that complex useless for our purposes). This suggests that the properties and deactivation pathways of the excited OER play the dominant role.

The laser experiments of this Section have provided an in-depth characterization of our electron sources on short timescales, from μs to ms. In the next Section, we will contrast them with LED photolyses, the durations of which are typically measured in hrs; nevertheless, the information they yield is largely equivalent, as we will show.

2.1.2 LED photolysis

The spectra of GS (SI–2.2) and OER (SI–2.4) show that the LED excites the same transitions as the laser did. The effective extinction coefficients with the polychromatic LED (for its spectrum, see SI–2.1) differ noticeably (SI–4.1) from the ones at the laser wavelength, which comes as a welcome side benefit in the case of GS.

The light intensity of our LED is 8 orders of magnitude lower than that of our laser during a pulse such that the tiny steady-state concentrations of $e^{\bullet-}_{aq}$ in preparative illumination require a quantification method other than direct observation. A viable alternative is provided by adding a substrate that does not interfere with the electron generator but scavenges $e^{\bullet-}_{aq}$ in a stoichiometrically defined reaction to give a stable product. The concentration of this accumulated product as function of the illumination duration is proportional to the total amount of $e^{\bullet-}_{aq}$ generated within that period; hence, its derivative is proportional to the $e^{\bullet-}_{aq}$ generation rate, that is, to the catalyst activity.

Chloroacetate ClAc is suited extremely well for this purpose: neither it nor its products

attack the catalyst; it quenches neither MLCT nor excited OER; but it reacts rapidly (rate constant, $1.9 \times 10^9\,M^{-1}s^{-1}$ at the high ionic strength of our samples) with $e^{\bullet-}_{aq}$.[8,9] The $e^{\bullet-}_{aq}$ capture is a dissociative electron transfer,[7]

$$ClCH_2COO^- \xrightarrow{+e^{\bullet-}_{aq}} Cl^- +^{\bullet} CH_2COO^- \xrightarrow{+H^{\bullet}} Cl^- + CH_3COO^- \qquad (2)$$

residual $HAsc^-$ can serve as the hydrogen donor for neutralizing the resulting carboxymethyl radicals, and the liberated chloride ion is inert. As a further asset, this reaction also represents an environmentally relevant application of $e^{\bullet-}_{aq}$ because ClAc is a bulk chemical (annual production in excess of 10^6 tonnes) with strong acute toxicity yet high persistence in the aquifer.[26]

In conjunction with the mechanism of Figure 1, Equation 2 thus suggests the formation of one chloride ion to be accompanied by the consumption of two ascorbate molecules. An ion-sensitive electrode provides a convenient means to measure the chloride concentration, and the ascorbate concentration can be selectively determined by using a chemical assay (SI–1). As the inset of Figure 3a demonstrates, there is indeed a fixed stoichiometric relationship between the two species over the whole conversion range; but the stoichiometric factor is somewhat smaller, namely, 1.6 in the case of RuBpy and 1.3 in that of RuDmb, which will emerge to be the least active and the most active of our catalysts. The discrepancy is caused by the partial involvement of the known[21] disproportionation of $Asc^{\bullet-}$ as a secondary reaction, which would recover one of the two ascorbate molecules if it occured quantitatively, but obviously none if it did not take place at all. The more active the catalyst is, the more $Asc^{\bullet-}$ it produces per unit time, increasing the disproportionation probability and thus lowering the ascorbate consumption. This behaviour on long timescales is consistent with the above-mentioned deceleration over time of the recombination between OER and $Asc^{\bullet-}$, which gains prominence at higher radical concentrations (SI–3.2).

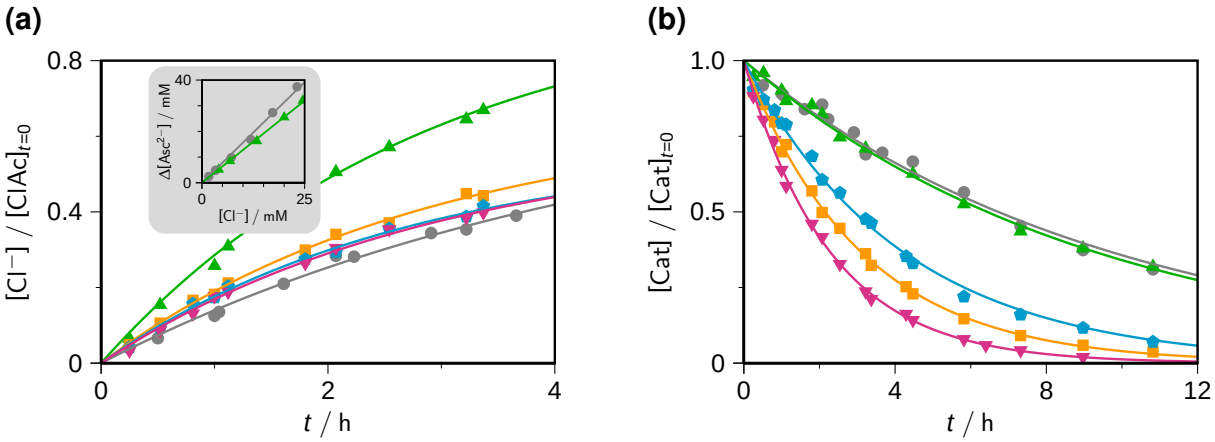

Figure 3: Full characterization of the electron sources of Figure 1 with the chloroacetate assay. Common experimental parameters, 50 μM catalyst, 75 mM Asc^{2-}, and 25 mM ClAc in 50 mM aqueous SDS at pH 12.7; colour codes and symbol shapes for the catalysts listed in Figure 2. Graph (a); time dependence of the chloride concentration liberated from ClAc, relative to the starting ClAc concentration (main plot), overlaid with best-fit functions $a(1 - \exp[-bt])$; and ascorbate consumption per chloride produced (inset) for the least and most active catalyst; slopes of the regression lines, 1.6 (RuBpy) and 1.3 (RuDmb). Graph (b), catalyst decomposition as function of the illumination time; overlaid with best-fit functions $\exp[-t/\tau_{Cat}]$. Further explanation, see text.

The main plot of Figure 3a displays the time dependence of ClAc decomposition according

10.1002/chem.201801955

to Equation 2 for our catalysts. Despite the deceptive simplicity of the curves, which can be approximated very well by monoexponential functions $a(1 - \exp[-bt])$ over the limited temporal range of the Figure, modelling the kinetics over the whole extent of the reaction is only possible numerically because the system composition changes in a nonlinear manner.[8] Fortunately, such an elaborate procedure is not at all necessary for comparing catalysts: instead, the desired information is already contained in the initial slopes of the curves, which correspond to the maximum generation rate of $e^{\bullet-}_{aq}$ for each system in its starting state, that is, with precisely known concentrations of all ingredients. These initial slopes directly yield (SI–4.2) the turnover frequencies for electron generation TOF($e^{\bullet-}_{aq}$), which describe the intrinsic activity of each catalytic system at the specified standard composition and irradiation conditions of this work. Table 2 lists their values, which clearly mark RuDmb as outstanding. Their connection with the photokinetic parameters obtained by laser flash photolysis will be discussed below.

Table 2: Comparison of the intrinsic performance of the investigated catalysts.

		RuBpy	RuDmb	RuTbb	RuMdnb	RuBdnb
TOF($e^{\bullet-}_{aq}$)	[h^{-1}]	78	170	113	106	100
τ_{Cat}	[h]	9.70	9.28	3.10	4.20	2.28
TON($e^{\bullet-}_{aq}$)		1510	3160	700	890	460

However, catalytic activity is only one side of the coin; the other, equally important one is catalyst stability. Figure 3b juxtaposes the decays of our catalysts, as measured through their luminescence (SI–1), during preparative illumination. They are represented very well by monoexponential functions $\exp[-t/\tau_{Cat}]$ with the lifetimes τ_{Cat} compiled in Table 2. The catalyst loss is thought to occur through thermal population of a dissociative dd state slightly higher in energy than MLCT.[27] This was recently corroborated by our investigation on the parent complex RuBpy,[8] which established that the decomposition rate is directly proportional to the LED power — and, by the same token, to the extinction coefficient of GS — as well as to the quenched lifetime of MLCT. However, in comparing different catalysts these trends can be totally obscured by the substance-specific efficiencies of ligand loss from the dd state, as the example of RuBpy and RuDmb shows. The energy gaps between their MLCT and dd states are 40 kJ/mol and 24 kJ/mol,[27] the effective extinction coefficient of GS with our LED (SI–4.1) is 50 % higher for RuDmb, and the lifetime of MLCT under our standard conditions (75 mM Asc^{2-}) is 70 % longer in the case of RuDmb. All these factors work in the same direction and should make RuDmb much less stable than RuBpy; yet, these two complexes possess values of τ_{Cat} that differ only by 5 % (Table 2). We ascribe this deviation from the expected trend to a lower dissociation tendency of the substituted ligand on account of its better σ-donating ability.

On the basis of the relationships that we have derived theoretically and demonstrated experimentally for the mechanism of Figure 1,[8,10] the influence of the chemical, spectroscopic,

and photokinetic parameters on TOF($e^{\bullet-}_{aq}$) is given by

$$\mathrm{TOF}(e^{\bullet-}_{aq}) \quad \propto \quad \sqrt{\varepsilon_{\mathrm{eff}}(\mathrm{GS}) \times [\mathrm{Cat}] \times \frac{K_{\mathrm{SV}} \times \eta}{k_{\mathrm{rec}}}} \times \varepsilon_{\mathrm{eff}}(\mathrm{OER}) \times \varphi_{\mathrm{ion}} \qquad (3)$$

Equation 3 is derived by setting up a steady-state approximation for OER and eliminating the intermediacy of MLCT through the quenching parameters.[8] At the low photon fluxes an LED delivers, both these simplifications incur negligible errors. The square root arises from the second-order recombination of OER and $Asc^{\bullet-}$ and applies to all processes except the ionization step.

The turnover number TON($e^{\bullet-}_{aq}$), which specifies the maximum amount of $e^{\bullet-}_{aq}$ a catalyst can deliver, comprises both the activity and the stability. As our systems do not exhibit catalyst poisoning, TON($e^{\bullet-}_{aq}$) can be estimated by[8]

$$\mathrm{TON}(e^{\bullet-}_{aq}) \quad = \quad 2 \times \tau_{\mathrm{Cat}} \times \mathrm{TOF}(e^{\bullet-}_{aq}) \qquad (4)$$

and the resulting values have been included in Table 2. Although they are only valid for the system composition (through [Cat] and K_{SV}) and irradiation conditions (through the $\varepsilon_{\mathrm{eff}}$(X) and τ_{Cat}) of this work, they still allow a performance comparison of the catalysts. It is seen that the highly lipophilic catalysts RuTbb, RuMdnb, and RuBdnb fall behind RuBpy by a considerable amount, contrary to the hopes that their higher lipophilicity would minimize k_{rec}, but that RuDmb clearly outranks the field.

Equation 3 is the central link between the experiments on short and long timescales provided that the catalyst concentration is kept constant and the ground-state spectra are known, requirements that are trivial to meet. Laser flash photolysis yields the OER spectra and the data of Table 1; and with these quantities, Equation 3 allows calculating relative values of TOF($e^{\bullet-}_{aq}$). Figure 4a demonstrates the success. Nevertheless, this approach has two inherent limitations. First, secondary reactions such as a disproportionation of the quencher-derived radicals can cause deviations; and there is little chance of extrapolating such effects from the timescale of laser flash photolysis to that of preparative photolysis. Ascorbate is not very critical in this respect, although the inset of Figure 3a indicates noticeable discrepancies, but with urate the disproportionation participates to such an extent that the square-root dependence no longer holds.[10] Second, the stability of our catalysts cannot be captured by laser flash photolysis because the decomposition quantum yields are too small to be measurable in pulsed experiments but become important through accumulating over the hours of the LED illumination.

When the reaction vessel has a larger diameter than the LED beam has, the question arises whether the beam should be magnified to fill the entrance window more completely but with lower intensity per area, or be collimated to illuminate only a small cylindrical subvolume but with higher intensity per area. Two opposite influences of this size change need to be considered. First, as long as the contents are continuously mixed by stirring, the only effect of partial illumination is a reduction of the overall excitation rates by the ratio of the illuminated volume to the total volume or, assuming a cylindrical vessel, by the corresponding area ratio of the beam and the entrance window.[14] Second, with the

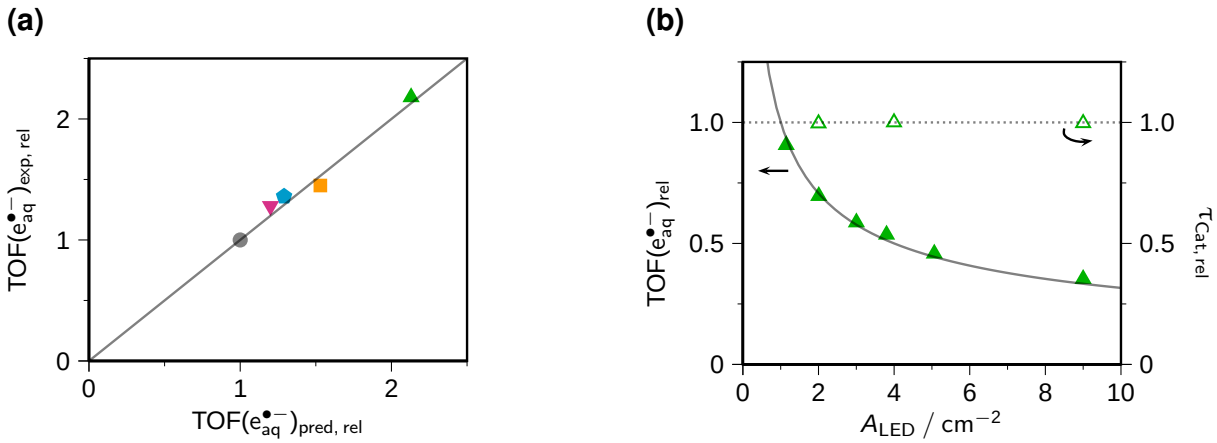

Figure 4: Predicting the activity and optimizing the performance of the catalytic electron sources for preparative LED photoredox catalysis. Catalyst colour codes and symbol shapes, see Figure 2. Graph (a), experimental turnover frequency TOF of electron production (Table 2) as function of the TOF calculated from the parameters obtained by laser flash photolysis (Table 1), both relative to the value for RuBpy. Graph (b), influence of collimating the LED to different areas A at constant power and solution volume on the electron generation rate TOF($e^{\bullet}_{aq}$) and the catalyst lifetime τ_{Cat}, both normalized to the values at an area of 1 cm^2. The arrows at the curves denote the pertaining vertical scale. Experimental parameters, 18 ml of 50 μM RuDmb, 75 mM Asc^{2-}, and 25 mM ClAc in 50 mM aqueous SDS at pH 12.7. TOF($e^{\bullet}_{aq}$), left scale, filled symbols, solid fit curve given by $\left(A_{LED}/(1\,cm^2)\right)^{-1/2}$; τ_{Cat}, right scale, open symbols, dotted constant line with height 1.0. Further explanation, see text.

mechanism of Figure 1 the rate of catalyst decay is directly proportional to the LED radiative power P, but the rate of electron generation or the associated quantity TOF($e^{\bullet}_{aq}$) exhibits the unusual dependence on $P^{3/2}$, as we have already verified experimentally.[8] Taken together, optically magnifying or reducing the beam diameter should not affect the catalyst stability in any way but should scale TOF($e^{\bullet}_{aq}$) with the inverse square root of the beam area.

Figure 4b tests these predictions and proves them to hold true, in particular, that for the electron generation rate, which might appear counterintuitive at first glance. In preparative work with the mechanism of Figure 1, concentrating the LED beam to the smallest possible diameter will thus give the best result.

2.2 Synthetic applications

RuDmb has the highest activity of our catalysts, yet — together with RuBpy — the longest lifetime under LED illumination; therefore, we carried out all the following syntheses with this complex. Its improved TOF($e^{\bullet}_{aq}$) can be exploited for shortening the irradiation duration or for increasing the amount of substrate. In this work we chose the second option, typically by doubling the substrate concentration compared to our previous work on RuBpy,[8] and occasionally also by upscaling the sample volume.

2.2.1 Dehalogenations

In Section 2.1.2, we have extensively used ClAc as a test compound for investigating the electron source of Figure 1 on the timescale of its applications. Here, ClAc additionally serves to demonstrate the feasibility of upscaling the reaction. To that end, we increased the solution volume by about an order of magnitude, from 3.8 ml to 36 ml, and partly

compensated the expected lengthening of the reaction time by doubling the optical path length, which approximately doubles the absorbed light because the solution is optically thin. As the NMR spectra in SI–5.1 bear out, near-quantitative turnover of the larger amount was achieved within 48 h.

The dehalogenation can also be employed to effect deuteration, and two of its features are very advantageous in that respect. First, the reaction is site-specific because the hydrogen atom takes the place of the chlorine atom. Second, it is easy and inexpensive; as the only requirement, one needs to work in D_2O instead of H_2O because the hydrogen (or deuterium) donor is the ascorbate, which exchanges all its transferable protons with the solvent. The upper traces of Figure 5a juxtapose the NMR spectra at the illumination end points for the two reaction media. The substrate is quantitatively dechlorinated in both cases, but the 1:1:1 triplet in the deuterated solvent evidences the conversion into CDH_2COO^-. The minute but clearly discernible singlet of CH_3COO^- at slightly lower field is larger than expected on the basis of the ascorbate weight-in concentration and the isotopic purity of the solvent, which suggests that the substrate and/or the SDS contribute as hydrogen donors to a small extent. Another deuteration example will be given below. The simplicity, selectivity, near-quantitative isotope substitution (as opposed to other methods in the literature)[28], and potentially large number of substrates that can be dechlorinated by $e^{\bullet-}_{aq}$ could make this an attractive method for deuteration and — with no changes in mechanism expected — tritiation, which is of importance for investigations of pharmaceuticals.[28–31] Using $e^{\bullet-}_{aq}$ as mediator seems to obviate the necessity of polarity matching by adding a thiol:[32] with the mechanism of this work, the ascorbate species efficiently serve as both the electron and the hydrogen-isotope donors in these photoredox-driven atom transfers.[31]

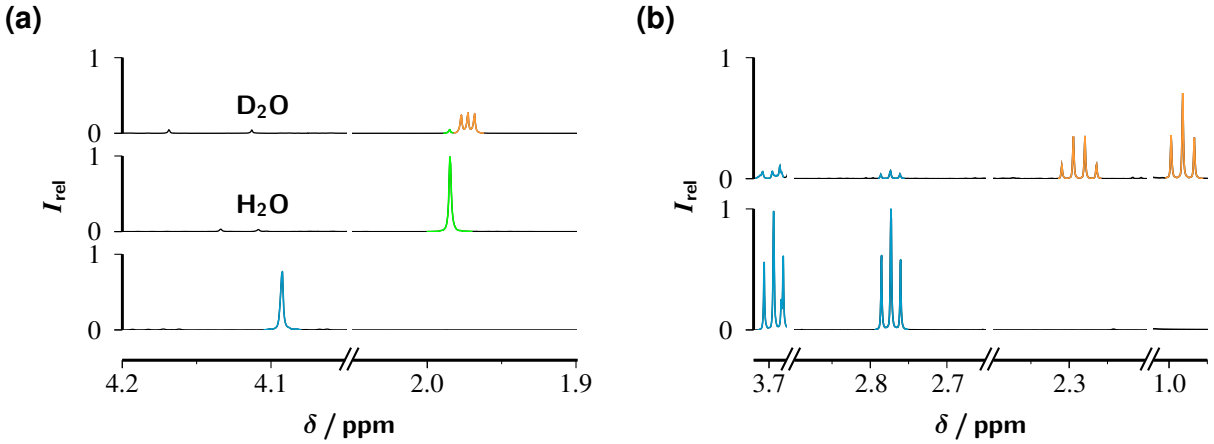

Figure 5: Dehalogenations of 10 mM aliphatic substrates with RuDmb and 75 mM Asc^{2-} in 50 mM aqueous SDS at pH 12.7. Shown are the ^{1}H-NMR spectra before (bottom traces) and after 14 h of illumination with the green LED (all other traces), with the NMR resonances of the respective substrate coloured cyan. Graph (a), chloroacetate ClAc in H_2O and D_2O, 50 μM RuDmb; products acetate (green, 1.98 ppm, s) and monodeuteroacetate (orange, 1.97 ppm, t 1:1:1). Graph (b), 3-chloropropionate ClPr, 100 μM RuDmb; product propionate (orange; 2.29 ppm, q; and 0.98 ppm, t). All spectra were recorded after acidification to pH 1; and each set of spectra has been normalized to the global maximum signal. Further explanation, see text.

As an even more demanding aliphatic substrate than ClAc, we selected 3-chloropropionate ClPr. The insertion of the sp^3 centre between the carbon atoms bearing the functional groups removes any through-bond activation of the C—Cl bond by the carboxylate substituent with respect to single-electron reduction. This is reflected by a more than threefold

decrease of the rate constant of electron capture (to $4.4 \times 10^8\,M^{-1}s^{-1}$, even lower than for 1-chloropropane)[7] compared to ClAc, which diminishes the fraction of $e_{aq}^{\bullet-}$ used productively. By doubling the catalyst concentration to 100 μM (1 mole%), however, we were able to convert ClPr to propionate with a yield of 90 % (Figure 5b), with the only cost incurred being a lower TON. This is consistent with our recent experiments on syntheses with a laser-driven catalytic $e_{aq}^{\bullet-}$ source, where we found $e_{aq}^{\bullet-}$ scavenging by $HAsc^-$ to be the underlying reason for a trade-off between maximizing either TON or substrate conversion.[9]

In contrast to aliphatic chlorides, chloroarenes lose halogen in a consecutive mechanism.[33] Their radical anions resulting from $e_{aq}^{\bullet-}$ capture live long enough for characterization before they cleave to give the chloride ion and a σ radical. For the monochlorinated benzoates *o*-ClBz, *m*-ClBz, and *p*-ClBz, the cleavage rate constants differ widely ($8 \times 10^7\,s^{-1}$, $1.2 \times 10^6\,s^{-1}$, and $4 \times 10^7\,s^{-1}$),[33,34] whereas the rate constants of $e_{aq}^{\bullet-}$ capture lie within a much more narrow range ($1.4 \times 10^9\,M^{-1}s^{-1}$, $4.8 \times 10^9\,M^{-1}s^{-1}$, and $6 \times 10^9\,M^{-1}s^{-1}$)[33]. Progressive scavenging of $e_{aq}^{\bullet-}$ by the reaction product benzoate (rate constant, $3.2 \times 10^9\,M^{-1}s^{-1}$)[7] complicates the kinetics but does not render the reaction self-limiting because the benzoate radical anion is thermodynamically capable of reducing the chlorinated substrates, which are less electron-rich than is benzoate.

We determined the dehalogenation yields given in Scheme 1 by the NMR spectra (SI–5.1), and in parallel also by measuring the chloride concentration, as in Section 2.1.2. Their trend reflects the interplay of $e_{aq}^{\bullet-}$ capture and radical-ion stability. Concentrating on the chlorine loss rather than on the stable end product benzoate is justified because it is equivalent to quantifying the formation of the highly reactive carboxyphenyl radicals, which can be used for cross coupling (see also below, Section 2.2.3).[10] The trapping of these radicals by a coupling product or by a hydrogen donor is strongly dependent on the concentration of the intercepting agent and on the structure of the substrate. Not unexpected for *o*-ClBz, the steric hindrance by the neighbouring carboxylate strongly suppresses additions of its carboxyphenyl radical to surplus substrate such that the only product is benzoate (see the spectrum in SI–5.1). With the other two isomers, the benzoate formation can be maximized by raising the concentration of the hydrogen donor $HAsc^-$ through lowering the pH to 11.6, concomitant with an increase of the ascorbate weight-in concentration such as to keep constant the Asc^{2-} concentration, and thus the TON($e_{aq}^{\bullet-}$); we have already demonstrated the feasibility of this strategy in our previous investigation with laser-generated $e_{aq}^{\bullet-}$.[9]

As the other examples of Scheme 1 show, the impressive reducing power of $e_{aq}^{\bullet-}$ makes these arene dehalogenations equally feasible in the case of 4-fluorobenzoate and 4-chlorophenylacetate. The latter compound no longer experiences the slight activation with respect to $e_{aq}^{\bullet-}$ capture that is caused by the direct attachment of the carboxylate substituent to the aromatic ring; to compensate for this, we had to halve the substrate concentration.

2.2.2 Hydrogenations of carbon–carbon double bonds

Olefinic double bonds are highly susceptible to attack by $e_{aq}^{\bullet-}$ (e.g., the rate constants for fumarate Fu and cinnamate Ci are $7.5 \times 10^9\,M^{-1}s^{-1}$ and $1.4 \times 10^{10}\,M^{-1}s^{-1}$).[7] Hence, the transformations of this Section are already complete within 6 h; and the yields of

10.1002/chem.201801955

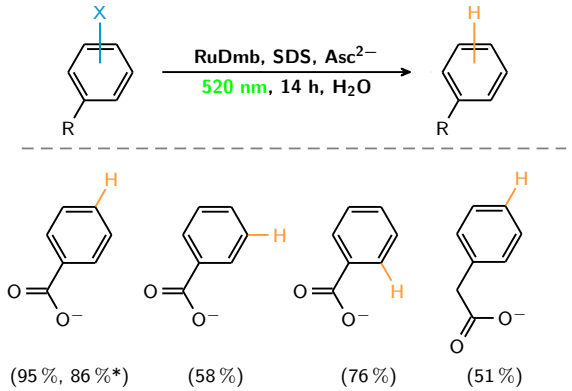

Scheme 1: Dehalogenation of aryl halides by $e^{\bullet-}_{aq}$ produced with an LED. Experimental conditions, 100 μM RuDmb and 75 mM Asc^{2-} in 50 mM aqueous SDS at pH 12.7; substrate concentrations, 5 mM (4-chlorophenylacetate) and 10 mM (all other compounds). The dehalogenation yields specified in parentheses pertain to the substrate with X in the position indicated by the orange H in the substitution product. Value with asterisk, X = F; all others, X = Cl. Further explanation, see text.

hydrogenated products are very good (Scheme 2 and SI–5.2). By control experiments with laser flash photolysis as in the right half of Figure 2a, but in the presence of the respective substrate, we ascertained that these reactions rely on the reducing power of $e^{\bullet-}_{aq}$ and cannot be effected by OER itself.

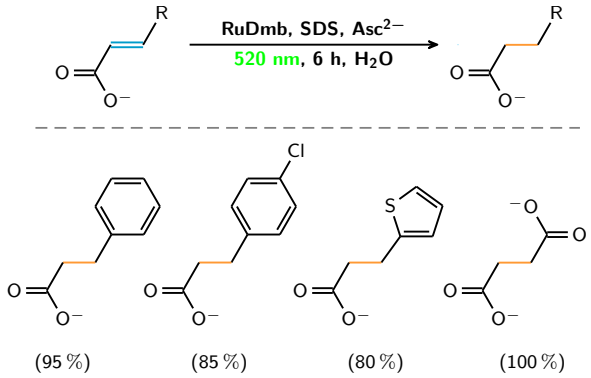

Scheme 2: Olefin hydrogenations via LED-generated $e^{\bullet-}_{aq}$. Experimental conditions, 100 μM RuDmb and 75 mM Asc^{2-} in 50 mM aqueous SDS at pH 12.7; substrate concentrations, 10 mM; yields given in parentheses. Further explanation, see text.

An example for the simultaneous presence of two substructures potentially transformable by $e^{\bullet-}_{aq}$ is provided by *p*-chlorocinnamate ClCi. Because the carbon–carbon double bond reacts much more readily with $e^{\bullet-}_{aq}$ than does an arylic carbon–chlorine bond, we anticipated that the double bond can be selectively hydrogenated while leaving unchanged the chlorinated ring; and Figure 6 demonstrates that this is indeed the case. As the only requirement, the illumination should not continue for too long after the olefinic substrate has been consumed, but this is not a crucial point as the initial product with an aliphatic side chain has about the same low reactivity towards $e^{\bullet-}_{aq}$ as has 4-chlorophenylacetate (compare Figure 5).

In analogy to ClAc (above, Figure 5a), deuterations of the olefinic bonds in ClCi and in its unsubstituted parent cinnamate are possible (top trace of Figure 6, and SI–5.2) simply by carrying out the reactions in D_2O. This is established by the aliphatic proton signals of the products in this medium, which exhibit the required halving of the integrals, a minute upfield

10.1002/chem.201801955

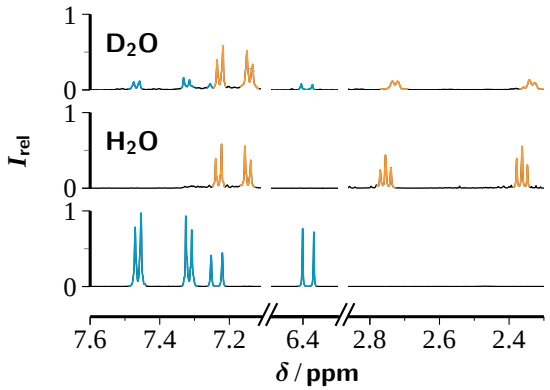

Figure 6: Addition of hydrogen or deuterium to the olefinic double bond of *p*-chlorocinnamate (10 mM) upon illumination with a green LED; catalytic system, 100 μM RuDmb and 75 mM Asc^{2-} in 50 mM aqueous SDS at pH 12.7; illumination duration, 6 h. Starting compound, cyan (aromatic protons at 7.47 ppm, d, and 7.32 ppm, d; olefinic protons at 7.24 ppm, d, and 6.39 ppm, d); product 3-(4-chlorophenyl)-propionate, orange (aromatic protons at 7.23 ppm, d, and 7.14 ppm, d; aliphatic protons in the protiated compound at 2.76 ppm, t, and 2.36 ppm, t; and in the deuterated compound at 2.73 ppm, d, and 2.33 ppm, d, both broadened by unresolved couplings to geminal and vicinal D). Bottom trace, ^{1}H-NMR spectrum before the illumination; centre and top traces, after the illumination in H_2O and D_2O. The vertical scales are identical. Further explanation, see text.

shift, and doublet patterns with the same coupling constant as in the protiated product; in contrast to ClAc, however, the couplings to deuterium cannot be resolved. We ascribe the somewhat lower yields for the additions of deuterium (ClCi, 80 %; cinnamate, 73 %) compared to those of hydrogen (Scheme 2) to the isotope effect for abstracting a deuterium or a hydrogen atom from the ascorbate monoanion. The slower abstraction in the case of deuterium increases the chance of deactivating the intermediate radical anion by back electron to the catalyst, that is, nonproductively.

2.2.3 Carbon–carbon bond formations

In line with expectation, and also corroborated by several of the examples in the preceding Sections, the final products and their yields reflect the competition between the different trapping reagents in the sample for the intermediate radicals or radical anions. The outstanding hydrogen-donating properties of $HAsc^-$ — whose presence in mM quantities is unavoidable when Asc^{2-} is the sacrificial electron donor in the catalytic $e^{\bullet-}_{aq}$ sources, unless the already strongly basic pH is raised to impractical values — causes a natural bias towards substitution by, or addition of, hydrogen. As we recently reported,[10] the replacement of ascorbate by urate can help circumvent this problem for the catalyst RuBpy; but this solution is not feasible with the other catalysts of this work because urate quenches their MLCT states much too inefficiently.

Here, we explore two other approaches that exploit the high activity of the catalyst RuDmb. With the first, we generate relatively stable radical anions in amounts sufficient for their dimerization to become competitive. With the second, we make use of the leeway this highly efficient catalyst provides us with, namely, by decreasing the Asc^{2-} concentration such that the $e^{\bullet-}_{aq}$ source still works but radical interception by $HAsc^-$ is minimized and the balance can be swung by a high concentration of another trapping agent.

Acetophenone AcPh illustrates the first strategy. This substrate captures $e^{\bullet-}_{aq}$ in a diffusion

10.1002/chem.201801955

controlled process (rate constant, $2.4 \times 10^{10}\,M^{-1}s^{-1}$)[7] but is inert towards OER of our ruthenium complexes[35] for thermodynamical reasons (the standard redox potential of AcPh is -1.8 V;[36] i.e., more negative than that of RuDmb by 0.73 V, compare Table 1). Once formed, the radical anions quantitatively undergo self-coupling.[37] Figure 7 evidences that our catalytic $e^{\bullet-}_{aq}$ source affords 2,3-diphenyl-2,3-butanediol as the only product and in excellent yield (see Scheme 3; and SI–5.3 shows of the successful upscaling of this experiment to ten times the volume). As the only modification of our standard procedure, we had to lower the SDS concentration to 30 % of its usual value because AcPh associates with the micelles, which would shield it from attack by $e^{\bullet-}_{aq}$. In accordance with the literature,[37] we found a dl:meso ratio of 54:46, confirming that the dimerization of the radical anions exhibits no significant diastereoselectivity. The value of our method lies in obviating the necessity of an expensive iridium catalyst for a pinacol coupling through photoredox catalysis;[35] our two-photon approach yields the same result with a much more affordable ruthenium catalyst, but can still be done with an LED.

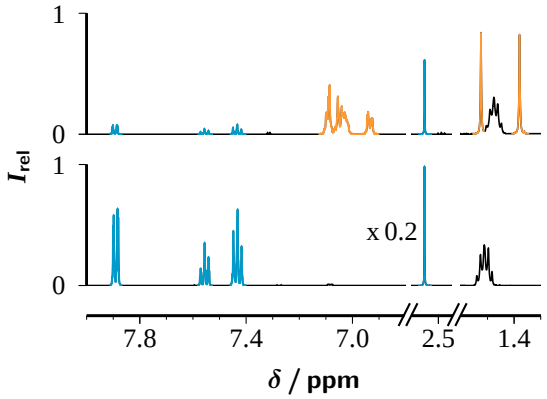

Figure 7: Homocoupling of acetophenone (10 mM), as effected by producing $e^{\bullet-}_{aq}$ with an LED. Catalytic $e^{\bullet-}_{aq}$ source, 100 μM RuDmb and 75 mM Asc^{2-} in 15 mM aqueous SDS at pH 12.7. Bottom trace, ^{1}H-NMR spectrum before the illumination; top trace, after illumination for 14 h. The vertical scales are identical. Starting compound, cyan (aromatic protons at 7.89 ppm, d, 7.55 ppm, t, and 7.43 ppm, t; aliphatic protons at 2.55 ppm, s, signal multiplied by 0.2 in the spectrum before irradiation); product 2,3-diphenyl-2,3-butanediol, orange (superposition of dl and meso forms for the aromatic protons at 7.09 ppm, d, 7.03 ppm, t, and 6.93 ppm, d; aliphatic protons of the dl form at 1.52 ppm, s; of the meso form, 1.38 ppm, s). The quintet of the SDS protons is shifted from 1.47 ppm in the starting spectrum to 1.47 ppm in the final spectrum because acetophenone and the diol associate differently with the micelles. Further explanation, see text.

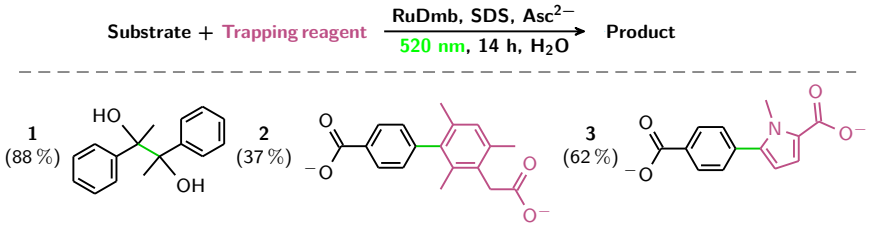

Scheme 3: Coupling reactions induced by $e^{\bullet-}_{aq}$ that are accessed through LED irradiation. Experimental conditions: 100 μM RuDmb and 75 mM / 30 mM (**1** / **2** and **3**) Asc^{2-} in 15 mM / 50 mM (**1** / **2** and **3**) aqueous SDS at pH 12.7; 10 mM / 5 mM (**1** / **2** and **3**) substrate; 200 mM trapping reagent (**2** and **3** only). The yields shown in parentheses were determined from the ^{1}H-NMR spectra (Figure 7 and SI–5.3). Further explanation, see text.

The examples of our second strategy employ the reactive carboxyphenyl radicals procured in high yields by dissociative $e^{\bullet-}_{aq}$ attachment to *p*-ClBz (Scheme 1). To push back their interception by hydrogen donation, we lowered the ascorbate weight-in concentration to

40 % of the standard concentration, which made it possible to add the desired trapping reagent in seventy-fold excess over $HAsc^-$ at pH 12.7. As trapping reagents that avoid the formation of several cross-coupling products, we selected mesitylacetate MesAc and *N*-methylpyrrole-2-carboxylate NMPCA. With the former, all ring positions except *meta* are occupied; with the latter, it is well known that the addition of radicals to pyrroles almost exclusively occurs at the ring position adjacent to the nitrogen atom.[38–43] Proof of principle for the viability of our approach is obtained from the NMR spectra in SI–5.3. In the case of MesAc, the deceleration of the traget reaction by the overcrowded trapping reagent only allows a moderate yield of the coupling product, with benzoate remaining the main product; however, the sterically less demanding NMPCA turns the table and approximately reverses the product distribution (Scheme 3).

On the basis of these results it can be concluded that for cross couplings via $e_{aq}^{\bullet-}$ a catalyst should be optimized with respect to both intrinsic activity and stability. RuDmb represents a step in that direction. The better the catalyst fares with respect to these properties, the more it will permit reducing the amount of sacrificial donor until the unwanted hydrogen abstraction by the substrate radicals becomes a minor side channel. This reduction decreases the $e_{aq}^{\bullet-}$ yield, hence is tantamount to systematic catalyst poisoning; but as long as the catalyst survives the proportionally larger number of excitations that are needed for the same turnover, the associated photophysical losses squander only photons but do not consume any chemicals.

3 Conclusions

The kinetic investigations of this work have juxtaposed a microscopic and a macroscopic strategy for characterizing our LED-driven catalytic $e_{aq}^{\bullet-}$ sources. Laser flash photolysis monitors the individual steps on the timescales associated with them, which typically means μs to ms; and we have shown that in its more sophisticated variant of two-pulse experiments it is capable of observing each key process of our complex mechanisms in isolation. Preparative LED kinetics with detection through a coupled transformation caused by $e_{aq}^{\bullet-}$ captures the time-integrated effect of all steps lumped together.

Both approaches have their specific strengths and weaknesses. From a practical perspective, the laser method needs special equipment as well as expertise and is very time-consuming, whereas the LED method uses the same setup as the actual syntheses, and the experiments are easy and fast to perform. On a fundamental level, the laser method provides direct and detailed information on practically all processes that determine the activity of a catalyst, which the LED method can only supply indirectly (through Equation 3) and with much more restricted possibilities of separating the influences.

This would make laser flash photolysis far superior were it not for two inherent limitations. First, it cannot properly characterize slow processes that play only a marginal role on fast timescales but may no longer be ignored during preparative illumination, such as the secondary chemistry of the radicals derived from the sacrificial donor. Second, it is blind to effects that are below the detection limit in pulsed experiments, where each absorbing

10.1002/chem.201801955

molecule is only excited once per pulse, but build up to large sum totals over the course of a preparative illumination, where the same molecule experiences a vast number of excitations: the catalyst decay falls into this category. In contrast, the LED kinetics is sensitive to both issues, and directly characterizes the second.

In summary, both methods overlap only to some extent and neither provides a complete picture; laser flash photolysis is indispensable when targeted improvement of the catalyst activity by structural modification is an aim, as in this work, but must always be complemented by the LED kinetics to determine the catalyst decay rate; when the focus is on optimizing the overall performance for reactions performed with the output of the catalytic system, investigating the LED kinetics as a stand-alone is both necessary and sufficient; and, in any case, the LED kinetics supplies much more detailed information on a transformation than does a single end-point measurement.

The remarkable fact that a low-power light source such as an LED can drive a two-photon process on a benchtop scale hinges on the feature that the chemically cached energy of the first photon ”leaks” only through a second-order process with respect to the intermediate. Utilizing the energy added by the second photon is by no means restricted to electron ejection: if the excited storage medium were instead quenched by an external species, the kinetics of product formation would still obey Equation 3 provided that φ_{ion} is replaced by the Stern–Volmer term pertaining to this quenching. Hence, all the dependences on process variables derived herein (e.g., on the light intensity; see Figure 4b) and previously[8,10] are of complete generality for any such two-photon processes.

The applications of $e_{aq}^{\bullet-}$ that we have presented illustrate that this ”super reductant” greatly extends the range of substrates that can be transformed. Owing to the composition of our catalytic $e_{aq}^{\bullet-}$ sources, the presence of mM concentrations of a good hydrogen donor is unavoidable. Through competition, this decreases the likelihood of self- and cross-couplings, although we have presented examples. However, substitutions of chlorine or fluorine by hydrogen as well as hydrogenations of double bonds are within easy reach. As a particular forte, the substrates can be deuterated selectively and with very high isotopic purity; and this feat can be performed in an extremely simple way: all that it takes is the replacement of the solvent H_2O by D_2O.

References

[1] J. M. R. Narayanam and C. R. J. Stephenson, *Chem. Soc. Rev.*, 2011, **40**, 102–113.

[2] C. K. Prier, D. A. Rankic and D. W. C. MacMillan, *Chem. Rev.*, 2013, **113**, 5322–5363.

[3] *Chemical Photocatalysis*, ed. B. König, DeGruyter, Berlin, 2013.

[4] D. Ravelli, M. Fagnoni and A. Albini, *Chem. Soc. Rev.*, 2013, **42**, 97–113.

[5] M. Reckenthäler and A. G. Griesbeck, *Adv. Synth. Catal.*, 2013, **355**, 2727–2744.

[6] N. A. Romero and D. A. Nicewicz, *Chem. Rev.*, 2016, **116**, 10075–10166.

[7] G. V. Buxton, C. L. Greenstock, W. P. Heiman and A. B. Ross, *J. Phys. Chem. Ref. Data*, 1988, **17**, 513–886.

[8] R. Naumann, F. Lehmann and M. Goez, *Angew. Chem. Int. Ed.*, 2018, **57**, 1078–1081.

[9] R. Naumann, C. Kerzig and M. Goez, *Chem. Sci.*, 2017, **8**, 7510–7520.

[10] R. Naumann and M. Goez, *Chem. Eur. J.*, 2018, DOI: 10.1002/chem.201800626.

[11] M. Goez, C. Kerzig and R. Naumann, *Angew. Chem. Int. Ed.*, 2014, **53**, 9914–9916.

[12] M. Brautzsch, C. Kerzig and M. Goez, *Green Chem.*, 2016, **18**, 4761–4771.

[13] T. Kohlmann, R. Naumann, C. Kerzig and M. Goez, *Photochem. Photobiol. Sci.*, 2017, **16**, 185–192.

[14] T. Kohlmann, R. Naumann, C. Kerzig and M. Goez, *Photochem. Photobiol. Sci.*, 2017, **16**, 1613–1622.

[15] S. Campagna, F. Puntoriero, F. Nastasi, G. Bergamini and V. Balzani, *Top. Curr. Chem.*, 2007, **280**, 117–214.

[16] S. P. Pitre, C. D. McTiernan and J. C. Scaiano, *Acc. Chem. Res.*, 2016, **49**, 1320–1330.

[17] R. Martinez-Haya, M. A. Miranda and M. L. Marin, *Eur. J. Org. Chem.*, 2017, 2164–2169.

[18] M. Marchini, G. Bergamini, P. G. Cozzi, P. Ceroni and V. Balzani, *Angew. Chem. Int. Ed.*, 2017, **56**, 2–4.

[19] A. Juris, V. Balzani, P. Belser and A. von Zelewsky, *Helv. Chim. Acta*, 1981, **64**, 2175–2182.

[20] H. B. Ross, M. Boldaji, D. P. Rillema, C. B. Blanton and R. P. White, *Inorg. Chem.*, 1989, **28**, 1013–1021.

[21] M. B. Davies, J. Austin and D. A. Partridge, *Vitamin C: Its Chemistry and Biochemistry*, The Royal Society of Chemistry, Cambridge, 1st edn., 1991.

[22] M. Goez, D. von Ramin-Marro, M. Schiewek and M. H. O. Musa, *Z. Phys. Chem. (Muenchen, Ger.)*, 2014, **228**, 193–207.

[23] R. McAlpine, M. Cocivera and H. Chen, *Can. J. Chem.*, 1973, **51**, 1682–1686.

[24] M. Goez and V. Zubarev, *Chem. Phys.*, 2000, **256**, 107–116.

[25] A. Juris, V. Balzani, F. Barigelletti, S. Campagna, P. Belser and A. von Zelewsky, *Coord. Chem. Rev.*, 1988, **84**, 85–277.

[26] M. Rossberg, W. Lendle, G. Pfleiderer, A. Tögel, E.-L. Dreher, E. Langer, H. Rassaerts, P. Kleinschmidt, H. Strack, R. Cook, U. Beck, K.-A. Lipper, T. R. Torkelson, E. Löser, K. K. Beutel and T. Mann, in *Ullmann's Encyclopedia of Industrial Chemistry*, Wiley-VCH Verlag GmbH & Co. KGaA, 2000.

[27] W. J. Dressick, J. Cline, J. N. Demas and B. A. DeGraff, *J. Am. Chem. Soc.*, 1986, **108**, 7567–7574.

[28] R. P. Yu, D. Hesk, N. Rivera, I. Pelczer and P. J. Chirik, *Nature*, 2016, **529**, 195–199.

[29] P. H. Allen, M. J. Hickey, L. P. Kingston and D. J. Wilkinson, *J. Label. Compd. Rad.*, 2010, **53**, 731–738.

[30] C. S. Elmore and R. A. Bragg, *Bioorg. Med. Chem. Lett.*, 2015, **25**, 167–171.

[31] Y. Y. Loh, K. Nagao, A. J. Hoover, D. Hesk, N. R. Rivera, S. L. Colletti, I. W. Davies and D. W. C. MacMillan, *Science*, 2017, **358**, 1182–1187.

[32] X. Guo and O. S. Wenger, *Angew. Chem. Int. Ed.*, 2017, **57**, 2469–2473.

[33] R. Zona, S. Solar, N. Getoff, K. Sehested and J. Holcman, *Radiat. Phys. Chem.*, 2008, **77**, 162–168.

[34] V. Konovalov, A. Raitsimring, Y. Tsvetkov and I. Bilkis, *Chem. Phys. Lett.*, 1989, **157**, 257–264.

[35] M. Nakajima, E. Fava, S. Loescher, Z. Jiang and M. Rueping, *Angew. Chem. Int. Ed.*, 2015, **54**, 8828–8832.

[36] G. J. Gores, C. E. Koeppe and D. E. Bartak, *J. Org. Chem.*, 1979, **44**, 380–385.

[37] S. Okamoto, K. Kojiyama, H. Tsujioka and A. Sudo, *Chem. Commun.*, 2016, **52**, 11339–11342.

[38] Y. M. Osornio, R. Cruz-Almanza, V. Jiménez-Montaño and L. D. Miranda, *Chem. Commun.*, 2003, 2316–2317.

[39] O. Guadarrama-Morales, F. Méndez and L. D. Miranda, *Tetrahedron Lett.*, 2007, **48**, 4515–4518.

[40] C. Iuga, S. O. Uribe, L. D. Miranda and A. Vivier-Bunge, *Int. J. Quantum Chem.*, 2010, **110**, 697–705.

[41] L. Marzo, I. Ghosh, F. Esteban and B. König, *ACS Catal.*, 2016, **6**, 6780–6784.

[42] J. I. Bardagi, I. Ghosh, M. Schmalzbauer, T. Ghosh and B. König, *Eur. J. Org. Chem.*, 2018, 34–40.

[43] M. Neumeier, D. Sampedro, M. Májek, V. A. de la Peña O'Shea, A. Jacobi von Wangelin and R. Pérez-Ruiz, *Chem. Eur. J.*, 2018, **24**, 105–108.

10.1002/chem.201801955

Table of contents entry

Add more life to years! A ligand substitution retains the light-stability of a micellized metal-complex Cat but boosts the activity of its ionizable form CAT for producing hydrated electrons $e_{aq}^{\bullet-}$ with a green LED, which are used for reductive transformations of otherwise unreactive substrates on a laboratory scale.